2022 International Conference on Multidisciplinary Research
https://doi.org/10.26803/MyRes.2022.21

Assessing the Effects of Material Properties on Load Behavior in Dry Ball Mills Using DEM

Fortune Nkomo
Gwanda State University,
Filabusi, Zimbabwe

Francois K. Mulenga
University of South Africa,
Johannesburg, South Africa

Abstract
Understanding how the mill load behaves is crucial for enhancing ball mill effectiveness. This study aimed to create a discrete element method (DEM) model to simulate the motion charge in ball mills and to analyze how the simulation material properties affected the load behavior. The steel balls were modelled as a collection of distinct particles, each of which was subject to Newton's laws of motion and tracked in a Lagrangian manner. Hertzian contact law was used to describe inter-particle collisions. Then, this numerical model was coded using the open-source C++ program LAMMPS Improved for General Granular and Granular Heat Transfer Simulation (LIGGGHTS) to mimic laboratory and pilot-scale ball mills. The load positions measured from the DEM simulations were compared to the published experimental data and empirical models of comparable laboratory and pilot-scale experiments to validate the findings. The angular shoulder position ranged between 137° to 154° for the range of Young's modulus of 0.5 to 1000 MN/mm^2. Angular shoulder and toe positions had a variation of less than 10% from the laboratory and pilot-scale experimental data. The outcomes demonstrated a significant relationship between load position and material characteristics such as Young's modulus in DEM simulation. This preliminary model can be used for choosing the appropriate material parameters for ball mills both with DEM and coupled CFD–DEM multiphase simulations. This assessment concluded that material properties affect the load behavior in computer simulations of ball mills.

Keywords: ball mill, computer simulation, discrete element modelling, LIGGGHTS, load position.

1. Introduction
Comminution refers to a set of operations widely used in the mining industry to fragment ore down to a sufficiently fine size. Comminution aims to liberate valuable minerals from waste constituents by breakage for easy subsequent beneficiation.

Various devices are employed at different stages of comminution. For example, jaw crushers and breakers are used at the primary stages, while ball mills are ubiquitously employed at the tertiary stages. Ball milling is indispensable not only in mineral processing but also in other industrial sectors. Power-generation and cement-manufacturing plants are good examples of where ball mills are used in the pulverization of rocks, clinker, and limestone to micro-sizes (Cleary, 2006). The mill is charged with ore-bearing rock and spherical steel balls. The mill is allowed to rotate around a central axis such that grinding takes place by collisions between freely moving balls and rock particles.

Comminution operations consume a substantial amount of energy and contribute significantly to the mine's electricity bill. Milling alone typically accounts for between 35% and 50% of the total mine operational costs. However, concordant studies have shown that less than 10% of the energy supplied to a ball mill is effectively spent on particle breakage. This demonstrates that milling is highly inefficient (Bouchard et al., 2017; Cleary 2001; Curry et al., 2014; Kelly & Spottiswood, 1982). It therefore becomes important to intimately understand the processes internal to a ball mill for its efficient operation so that slight adjustments in ball mill designs and operation result in meaningful cost savings.

There are two broad approaches to studying the internal micro- and macro-processes taking place inside a ball mill: experimentation and computer-based engineering simulation. The experimental approach involves the use of laboratory, pilot, and full-scale ball mills for data collection. One advantage of experimentation is that actual measurements are taken under well-controlled operating conditions for enquiry. The problem, however, is that experimental testing requires costly measurement instruments that are expected to function in and around the aggressive milling environment. Computer-based engineering simulation can be used to gain insight into a ball mill at a fraction of the costs of experimental testing. Engineering simulation has been an integral part of ball milling research (Broseghini et al., 2016; Chenje, 2009; Cleary et al., 2006; Mori et al., 2004). Its main shortcoming is the need to calibrate the simulation model before it can be used. This calibration process is iterative and demanding yet necessary before simulation outputs are deemed valid.

When developing a computer-based simulator, material properties play a key role in the performance of the simulator. Properties such as coefficient of restitution, and friction may impact the final behavior of simulated material. The coefficient of restitution has also been found to have a bearing on milling simulations (Boemer & Ponthot, 2017). On the other hand, varying Young's modulus does not affect the bulk flow behavior of the granular material. However, varying its value changes the computational times enormously (Van Lew et al., 2015; Yan et al. 2015). It is still not clear how the choice of material properties affects the load behavior of a simulated ball mill.

The purpose of this research was to develop a computer code capable of simulating the load behavior of a dry ball mill using an open-source package and to assess the

influence of various material properties on the dynamic load behavior. To address this challenge, dry milling was simulated using an open-source discrete element method (DEM) solver, and data on load position were compared to published experimental results. Experimental data from laboratory and pilot mills were used to validate the computer-based simulation model. This data and associated details on their collection were sourced from research articles (Katubilwa, 2013; Katubilwa & Moys, 2011; Mulenga, 2020; Mulenga & Bwalya, 2019; Mulenga & Moys, 2014).

2. Numerical modelling of a dry mill

DEM, a set of numerical techniques extensively used in modelling particulate systems, was applied to model the dynamic behavior of grinding media (Jahani, 2019; Jayasundara & Zhu 2022; Mhadhbi, 2021; Mishra & Rajamani, 1990, 1992; Radiszewski, 1999; Rajamani, 2000). The behavior of grinding media was modelled using the soft-sphere approach, which closely represents the practical behavior of the mill charge as compared to the hard-sphere formulation. Each ball was treated as a distinct particle, governed by Newton's Second Law of Motion applied at the center of mass of each particle (Equation (1). Euler's Second Law of Motion was used to describe changes in angular momentum (Equation (2). In terms of describing the motion of balls in the ball milling system, the dense charge was assumed to experience long and multiple contacts between particles. Based on this, the DEM model was built around three assumptions. First, particles retain their original shape after a collision. Second, collisions are inelastic, instantaneous, and repulsive. Finally, collisions occur between a pair of particles at any point in time.

$$F_i = m_i d\overrightarrow{v_i} = m_i \frac{d^2\vec{x}_i}{dt^2} = \sum_{j=CL_i} \vec{f}_{ij}^{\,p-p} + \vec{f}_i^{ext} \quad (1)$$

$$I_i d\overrightarrow{\omega_i} = I_i \frac{d^2\vec{\omega}_i}{dt^2} = \sum_{j\in CL_i} \left(\vec{M}^t{}_{ij} + \vec{M}^r{}_{ij}\right) for\ j = 1, \ldots, N \quad (2)$$

Where $\vec{f}_{ij}^{\,p-p}$ is the sum of different forces that act on the particle i;
x_i is the particle position;
v_i is the translational velocity of the particle.

Where $\sum_{j=CL_i} \vec{f}_{ij}^{\,p-p}$ is the sum of particle–particle interaction forces acting on particle i;
$\vec{f}_i^{ext}$ is forces acting on particle i due to external fields, such as gravitational, magnetic, or electromagnetic forces;
$\vec{M}^t{}_{ij}$ represents tangential torque, produced by particle–particle collision;
$\vec{M}^r{}_{ij}$ stands for rolling friction acting on particle i.

Interaction forces were assumed to obey the Hertzian contact law, whereby each particle interacts with nearby particles through particle-particle contacts which are

formed or broken at each timestep (Chegeni, 2018). Consider two particles of radii R_i and R_j that are approaching each other moving at velocities v_i and v_j, as shown in Figure 1. Upon collision, they deform by a distance equivalent to their supposed overlap, as illustrated in Figure 1(c). The collision force is related to the normal (δ_n), tangential overlap (δ_t) and the relative velocity of particles (v_{rn}) by the proportionality factor of spring stiffness (k_n) (Goniva et al., 2010). The contact force is expressed by Equation (3):

$$\vec{f}_{ij} = (k_n \delta_n)\vec{n}_{ij} - (\eta_n v_{rn})\vec{n}_{ij} + (k_t \delta_t \vec{t}_{ij} - (\eta_t v_{rt})\vec{t}_{ij} \qquad (3)$$

Where k_n and k_t are the normal and tangential spring constants of linear spring, as defined by Di Renzo and Di Maio (2004), and η_n and η_t are the normal and tangential linear velocity damping coefficients;
v_{rn} and v_{rt} are the normal and tangential components of relative velocity;
$\vec{n}_{ij}$ and $\vec{t}_{ij}$ are the normal and tangential vectors between the centers of particles i and j.

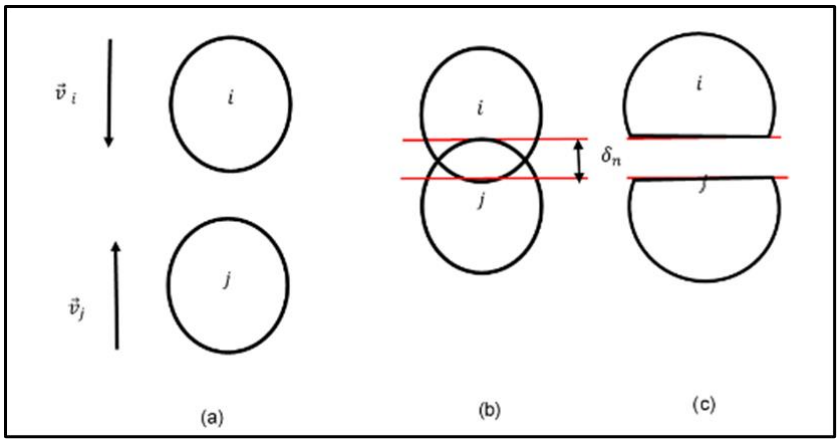

Figure 1: Particle contact and overlap: (a) particles approaching, (b) particles colliding and overlapping, and (c) deformed particles on contact

2.1 DEM input parameters

The material contact properties, such as Young's modulus, coefficient restitution, coefficient of friction, and the timestep, were varied, as shown in ***Table 1***.

Table 1: Material properties

Material property	**Range**
Young's modulus (E) (N/mm^2)	0.50 – 1000
Poisson's ratio (v_m)	0.03 – 0.30
Coefficient of restitution (e_n)	0.005 – 0.90
Sliding friction coefficient (μ_s)	0.005 – 0.90
Rolling friction coefficient (μ_r)	0.01 – 1

In the simulations, the grinding media and mill parts were separately assigned material property values. This was done so that the properties of the mill material and grinding media could be varied independently. Ranges for the Young's modulus and

Poisson's ratio were established based on the assumption that the particles follow a soft-sphere modelling approach and recommended values used in similar studies (Chengeni, 2018; Mayank et al., 2015; Smuts, 2015). Typical properties of grinding media can be found in studies by Aldrich (2013) and Massola et al. (2016). Simulations were performed to determine the effects of varying each parameter on the load position.

2.2 Selection of timestep

Particle movement in dense multiphase systems is not only affected by neighboring particles but also by distant particles (Smuts, 2015; Zhu et al., 2007). The Rayleigh method (Equation 4) was used to compute the critical timestep size (t_R). The Rayleigh timestep is solely dependent on the particle properties, and thus will remain constant during the simulation for a given set of particle properties, simplifying the computation process (Kremmer & Favier, 2001). A numerical timestep of 0.2 t_R was applied in the simulations. This size of timestep allowed the disturbance to propagate between immediate neighboring particles only (Cundall & Strack, 1979; Li et al., 2005).

$$t_R = \frac{\pi r_i}{(0.1631\nu_i + 0.8766)}\sqrt{\frac{\rho_i}{G_i}} \tag{4}$$

Where G_i is the shear modulus of the particle given by:

$$G_i = \frac{Y_i}{2(\nu_i + 1)} \tag{5}$$

Here, ν_i is the Poisson's ratio, Y_i the Young's modulus, and ρ_i the density of the particle.

2.3 Experimental conditions for DEM simulations

Figure 2 depicts snapshots of the laboratory and pilot mills and their respective rendering.

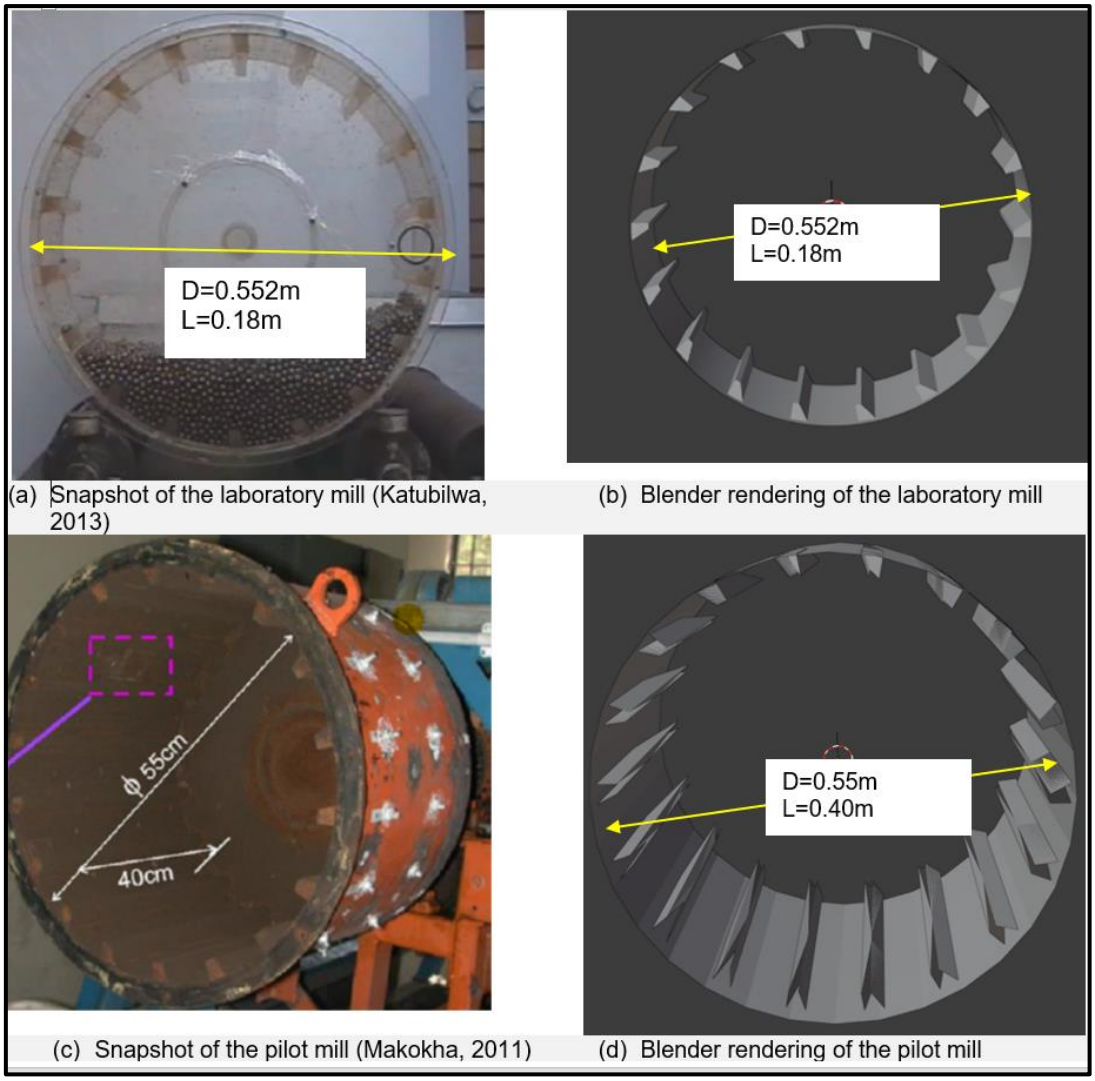

Figure 2: Rendering of mill geometries

2.4 Procedure

Simulations were run using a custom virtual Linux®-based, Ubuntu 20.04 LTS machine hosted on a Windows® Dell Precision M6700 personal computer, with Intel® Core (TM) i7-3740QM Quad (four-core), 8 logical processers, 2.4 GHz, and 16 GB RAM. The mill geometry was developed using Blender version 2.9, an open-source and CAD software. The files were then exported as .stl format and read into LIGGGHTS for simulation purposes. Converting the Blender files to .stl files has the advantage that this format describes the surface geometry only. Attributes common to other CAD models, such as color, texture, and material types, are not represented in the .stl file of this mill. This feature also allows one to set suitable material properties for various scenarios under investigation in the input script. LIGGGHTS, an open-source DEM solver, was used to simulate the dry milling experiments.

Mill set up and experimental conditions provided by Katubilwa (2013) using the pilot and laboratory mills were used as a basis for the simulation conditions. Dimensions of the mills and experimental conditions are presented in Figure 2. The pilot mill was loaded with grinding media balls, and the mill speed was then varied from 24.6% to

106.1% critical. To assess the influence of DEM input parameters on the behavior of the mill charge, material properties were varied one at a time and the shoulder and toe angular positions recorded. These simulations were performed at 20% ball filling and mill speed of 67% critical.

3. Results and discussion

The toe and shoulder angular positions were measured with 12 o'clock position as 0° in an anticlockwise direction, as shown in Figure 3.

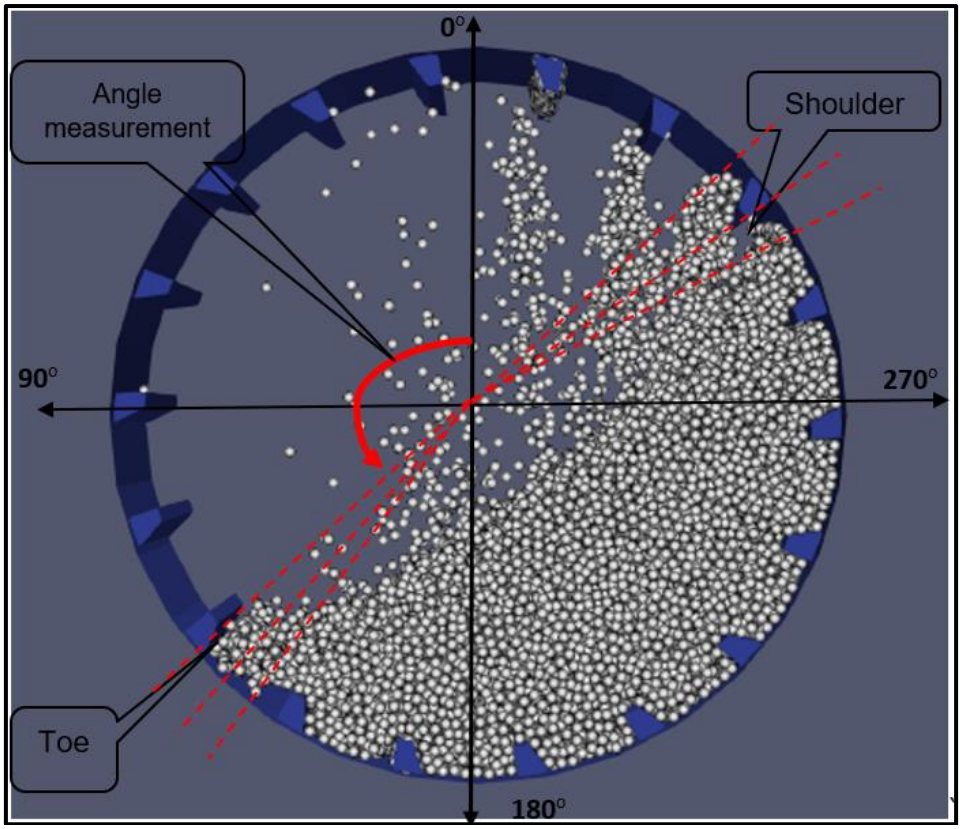

Figure 3: Pictorial depiction of shoulder and toe position measurement

In this study, Young's modulus was varied, while all other material properties (i.e., friction coefficient) and operational factors (e.g., mill speed, ball filling, and lifter configuration) were held constant. The lower limit and the upper limit were chosen to be 0.5 and 1000 MN/mm², respectively. These values were guided by the acceptable Young's modulus limits for the soft-sphere approach used in this work. A LIGGGHTS value above 1000 MN/mm² automatically assigns the hard-sphere approach to the simulation. Varying the Young's modulus influences the choice of the timestep for a particular simulation, as presented in Equations (4) and (5). To maintain the stability of the simulations, a different timestep had to be selected for simulations at Young's modulus greater that 500 MN/mm². Table 2 shows the variation of the Young's modulus on the Raleigh times (t_R), 20% of Raleigh times ($0.2t_R$), the selected timestep, and measured shoulder and toe positions.

Table 2: Effects of varying Young's modulus on Raleigh, simulation times, size of timesteps, and angular load position

Young's Modulus (MN/mm²)	t_R**(s)**	$0.2t_R(s)$	**Timestep (s)**	**Simulation time (s)**	**Lab mill**		**Pilot mill**	
					$\theta_T(^o)$	$\theta_S(^o)$	$\theta_T(^o)$	$\theta_S(^o)$
0.5	0.0067	0.0013	0.0001	1792.4	137.3	294.4	136.1	296.3
5	0.0021	0.00042	0.0001	1806.1	149.1	298.6	147.3	297.5
500	0.0007	0.00013	0.0001	2712.5	149.5	298.7	148.7	310.8
5000	0.0002	0.00004	0.00001	6816.6	153.3	303.5	155.2	305.6
1000	0.0002	0.00004	0.00001	6603.5	154.6	302.9	154.8	307.6

From Table 2 it can be observed that increasing the Young's modulus results in an increase in the Raleigh times. For values of Young's modulus between 0.5 and 500 MN/mm², a timestep of 0.0001 s was chosen, because it is within the recommended $0.2t_R$ (Norouzi et al., 2016). Decreasing the timestep increased the overall simulation times. At 0.5 MN/mm², it took about 30 minutes to run a simulation, while at 1000 MN/mm², about 2 hours to complete the simulation.

3.1 Effects of Young's modulus on the angular load position

The results presented in Table 2 show that both the toe and shoulder angles slightly increased with increasing Young's modulus for both laboratory and pilot mills. The toe angular position increased from about 137° to 155° as the modulus of elasticity was varied from 0.5 to 1000 MN/mm². On the other hand, the shoulder position increased from 296° to 310° and then decreased when the modulus of elasticity values were increased beyond 50 MN/mm².

The results support the theory that material properties affect the behavior of a DEM-simulated dry mill. First, the results showed that the modulus of elasticity affects the choice of timestep and overly the simulation time. This happens because when one decreases the timestep, more computational steps are performed for a specified time period. Thus, the choice for the Young's modulus is a trade-off between computational time and the accuracy of the simulation. To economically manage computational times, each simulation run was allocated a maximum of 2 hours. This provided guidance in selecting the suitable timestep, thus modulus of elasticity. Furthermore, during the study, it was observed that the Young's modulus value must be set reasonably close to that of the actual material and a critical value. This critical value is the point at which the results of the model deviate significantly from reality (Zhai et al., 2020). Typically, grinding steel balls has a modulus of elasticity ranging from 0.35 to 0.55 MN/mm², which is why selecting a value closer to the true material value makes much sense.

3.2 Effects of coefficient of friction on load position

The effects of the rolling friction coefficient (μ_r) and sliding friction coefficient (μ_s) on the load position were assessed. The coefficient of rolling friction is dependent on the radius of the rolling object, deformation of the grinding media, and the toughness of the surface. Rolling friction, on the other hand, takes place when an object rolls on a surface. In this light, the effect of the rolling friction coefficient (μ_r) was assessed in the DEM simulation using the pilot mill shell. Similar conditions of 20% ball filling and 67% of the mill critical speed were applied. Increasing μ_r results in a corresponding increase in the angular load position. When torque is applied to a stationary mill charge, static rolling friction holds back the charge motion. When μ_r increases, this resistive force that slows down the motion of rolling charge also increases. This explains this trend shown in Figure 4(a).

The coefficient of sliding friction (μ_s) varied from 0.005 to about 1.5. The shoulder position increased from 285° to 323°. There was a notable bump when the values of μ_s were 0.1 and 0.5 for both the shoulder and toe positions. This might be an indicator that there is a significant frictional force acting on the grinding media. This increased resistance to sliding results in media sticking to the mill shell. In general, increasing the value of μ_s results in an increase in the shoulder and toe positions. At very low values of μ_s, around 0.005 slip conditions exist because the mill charge slips and remains almost stationary when the mill rotates. It becomes impossible to measure the toe and shoulder positions at such low values.

3.3 Effects of coefficient of restitution on load position

The values of the coefficient of restitution (e_n) were systematically varied from 0.001 to 1 and the effect of this variation on the load position was assessed. Figure 4(c) illustrates the results obtained from this simulation. The coefficient of restitution seems not to have had any meaningful influence on the angular position. The load angular position remained constant between 250^o and 256^o for the shoulder and between 157^o and 163^o for the toe. The solid line with crosses indicates that changing the coefficient of restitution statically does not affect the angular load position. Thus, the value 0.6 for e_n was selected. This value is similar to the coefficient of restitution for the actual steel balls. Similar studies have recommended a value of between 0.4 and 0.75 (Dong & Moys, 2002; Katubilwa, 2013; Mishra & Rajamani, 1992).

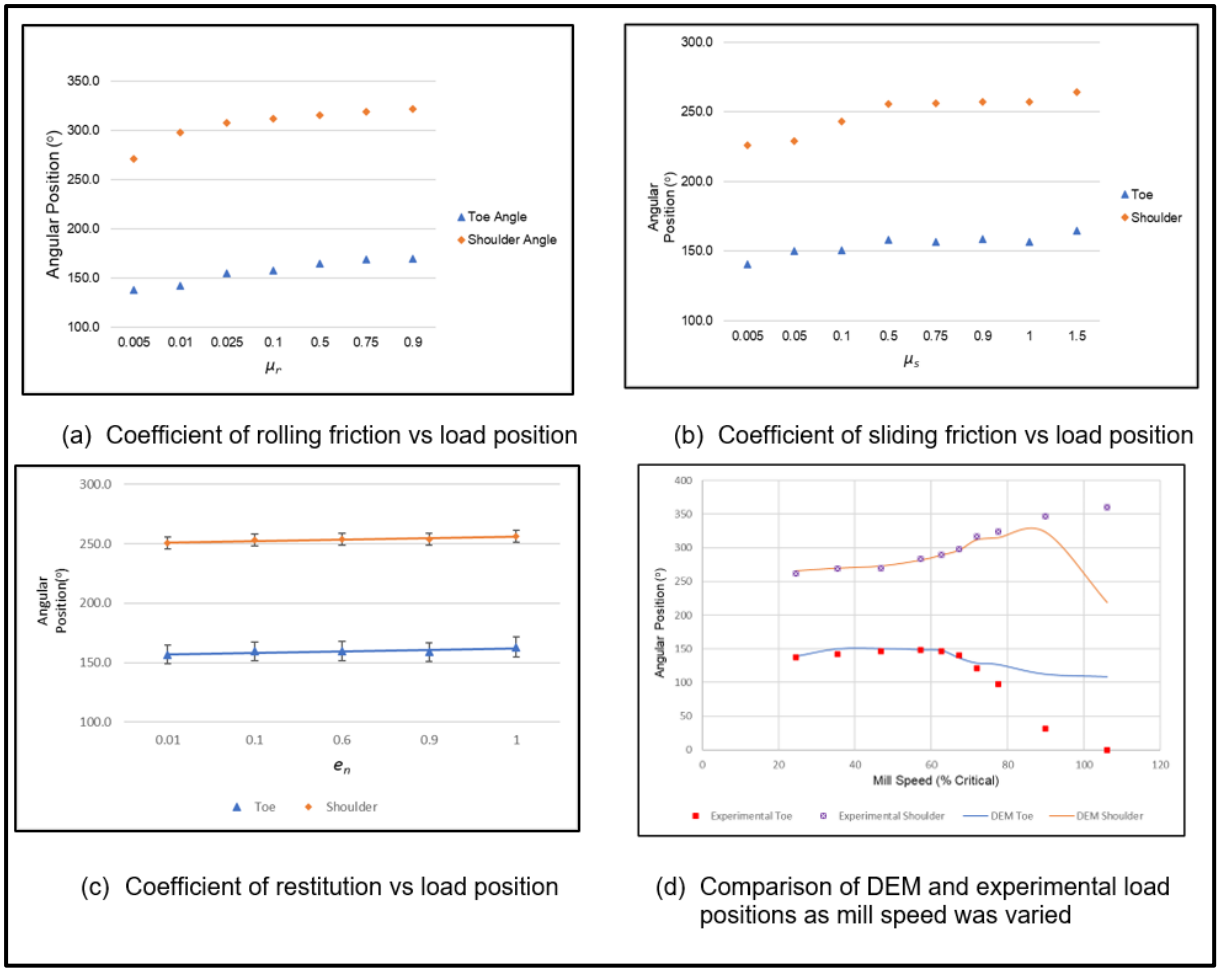

Figure 4: Comparison of DEM simulation and experimental shoulder and toe positions as mill speed was varied

4. Conclusions

Angular load position was compared with data from pilot and laboratory mill experiments. In this study, material properties were also accessed to determine their effects on the load position. The methodology for the development of a DEM numerical model for the dry mill was described. The model was tested to assess its behavior concerning the load behavior of a dry mill. The results from the DEM simulation are a good fit for laboratory and pilot-scale experiments. Accurate representations of the known dry milling conditions were achieved even though deviations from experimental data were observed at high mill speeds. The preliminary behavior of the DEM model is reasonable and follows some good trends. However, work still needs to be done to refine it further. In particular, the effects of various contact models on load behavior still need to be fully explored. Once the development and validation of the model have been completed, it will provide interesting insights into the load behavior of dry mills and provide a platform to explore the load behavior in wet ball mill environments.

5. References

Aldrich, C. (2013). Consumption of steel grinding media in mills: A review. *Minerals Engineering, 49*, 77–91. https://doi.org/10.1016/j.mineng.2013.04.023

Boemer, D., & Ponthot, J.-P. (2017). DEM modelling of ball mills with experimental validation: Influence of contact parameters on charge motion and power draw. *Computational Particle Mechanics, 4*, 53–67. https://doi.org/10.1007/s40571-016-0125-4

Bouchard, J., LeBlanc, G., Levesque, M., & Radziszewski, P. (2017). *Breaking down energy consumption in industrial grinding mills* [Conference session]. Canadian Mineral Processors Conference. Ottawa, Ontario.

Broseghini, M., Gelisio, L., D'Incau, M., Azanza Ricardo, C. L., Pugno, N. M., & Scardi, P. (2016). Modelling of the planetary ball-milling process: The case study of ceramic powders. *Journal of the European Ceramic Society, 36*(9), 2205–2212. https://doi.org/10.1016/j.jeurceramsoc.2015.09.032

Chegeni, J. M. (2018). Combined DEM and SPH simulation of ball milling. *Journal of Mining and Environment, 10*(1), 151–161. https://doi.org/10.22044/jme.2018.7363.1587

Chenje, T. P. (2009). *Steel media wear: Experimentation, simulation and validation* [Conference session]. 41st Annual Canadian Mineral Processors Conference. Ottawa.

Cleary, P. (2001). Modelling comminution devices using DEM. *International Journal for Numerical Analysis Methods in Geomechanics, 25*, 83–105. https://doi.org/10.1002/1096-9853(200101)25:1<83::AID-NAG120>3.0.CO;2-K

Cleary, P. W. (2006). Axial transport in dry ball mills. *Applied Mathematical Modelling, 30*, 1343–1355. https://doi.org/10.1016/j.apm.2006.03.018

Cleary, P. W., Sinnott, M., & Morrison, R. (2006). Prediction of slurry transport in SAG mills using SPH fluid flow in a dynamic DEM based porous media. *Minerals Engineering, 19*(15), 1517–1527. https://doi.org/10.1016/j.mineng.2006.08.018

Cundall, P. A., & Strack, O. D. L. (1979). A discrete numerical model for granular assemblies. *Géotechnique, 29*(1), 47–65. https://doi.org/10.1680/geot.1979.29.1.47

Curry, J., Ismay, M., & Jameson, G. (2014). Mine operating costs and the potential impacts of energy and grinding. *Minerals Engineering, 56*, 70–80. https://doi.org/10.1016/j.mineng.2013.10.020

Di Renzo, A., & Di Maio, F. P. (2004). Comparison of contact-force models for the simulation of collisions in DEM-based granular flow codes. *Chemical Engineering Science, 59*(3), 525–541. https://doi.org/10.1016/j.ces.2003.09.037

Dong, H., & Moys, M. H. (2002). Measurement of impact behaviour between balls and walls in grinding mills. *Minerals Engineering, 16*(6), 543–550. https://doi.org/10.1016/S0892-6875(03)00057-8

Jahani, C. (2019). Combined DEM and SPH simulation of ball milling. *Journal of Mining and Environment, 10*, 151–161. https://doi.org/10.22044/jme.2018.7363.1587

Jayasundara, C. T., & Zhu, H. P. (2022). Impact energy of particles in ball mills based on DEM simulations and data-driven approach. *Powder Technology, 395*, 226–234. https://doi.org/10.1016/j.powtec.2021.09.063

Katubilwa, F. M. (2013). *Effects of pool volume on wet milling efficiency* [PhD thesis]. University of the Witwatersrand, Johannesburg.

Katubilwa, F. M., & Moys, M. H. (2011). Effects of filling degree and viscosity of slurry on mill load orientation. *Minerals Engineering, 24*(13), 1502–1512. https://doi.org/10.1016/j.mineng.2011.08.004

Kelly, E. G., & Spottiswood, D. J. (1982). *Introduction to mineral processing*. John Wiley & Sons.

Kremmer, M., & Favier, J. F. (2001). A method for representing boundaries in discrete element modelling—part II: Kinematics. *International Journal for Numerical Methods in Engineering, 51*(12), 1423–1436. https://doi.org/10.1002/nme.185

Li, Y., Xu, Y., & Thornton, C. (2005). A comparison of discrete element simulations and experiments for "sandpiles" composed of spherical particles. *Powder Technology, 160*(3), 219–228. https://doi.org/10.1016/j.powtec.2005.09.002

Makokha, A. B. (2011). *Measuring, characterization and modelling of load dynamic behaviour in a wet overflow-discharge ball mill* [PhD thesis]. University of the Witwatersrand, Johannesburg.

Massola, C. P., Chaves, A. P., & Albertin, E. (2016). A discussion on the measurement of grinding media wear. *Journal of Materials Research and Technology, 5*(3), 282–288. https://doi.org/10.1016/j.jmrt.2015.12.003

Mayank, K., Malahe, M., Govender, I., & Mangadoddy, N. (2015). Coupled DEM–CFD model to predict the tumbling mill dynamics. *Procedia IUTAM, 15*, 139–149. https://doi.org/10.1016/j.piutam.2015.04.020

Mhadhbi, M. (2021). Simulation of a laboratory scale ball mill via discrete element method modelling. *Advances in Materials Physics and Chemistry, 11*(10), 167–175. https://doi.org/10.4236/ampc.2021.1110016

Mishra, B. K., & Rajamani, R. K. (1990). Motion analysis in tumbling mills by the discrete element method. *Kona Powder and Particle, 8*, 92–98. https://doi.org/10.14356/KONA.1990016

Mishra, B. K., & Rajamani, R. K. (1992). The discrete element method for the simulation of ball mills. *Applied Mathematical Modelling, 16*(11), 598–604. https://doi.org/10.1016/0307-904X(92)90035-2

Mori, H., Mio, H., Kano, J., & Saito, F. (2004). Ball mill simulation in wet grinding using a tumbling mill and its correlation to grinding rate. *Powder Technology, 143–144*, 230–239. https://doi.org/10.1016/j.powtec.2004.04.029

Mulenga, F. K. (2020). Towards a pool-based model of volumetric slurry hold-up for cylindrical ball mills. *Mineral Processing and Extractive Metallurgy Review, 41*(4), 227–239. https://doi.org/10.1080/08827508.2019.1635471

Mulenga, F. K., & Bwalya, M. M. (2019). Determination of the formal powder filling of a wet ball mill in open circuit configuration. *Minerals Engineering, 130*, 1–4. https://doi.org/10.1016/j.mineng.2018.10.004

Mulenga, F. K., & Moys, M. H. (2014). Effects of slurry filling and mill speed on the net power draw of a tumbling ball mill. *Minerals Engineering, 56*, 45–56. https://doi.org10.1016/j.mineng.2013.10.028

Norouzi, M. N., Sotudeh-Gharebagh, H. R., & Zarghami, R. (2016). *Coupled CFD–DEM modeling: Formulation, implementation and applications to multiphase flows*. John Wiley & Sons.

Radziszewski, P. (1999). Comparing three DEM charge motion models. *Minerals Engineering, 12*, 1501−1520. https://doi.org/10.1016/S0892-6875(99)00137-5

Rajamani, R. K. (2000). Semi-autogenous mill optimization with DEM simulation software. In J. Herbst (Ed.), *Control 2000: Mineral and metallurgical processing* (pp. 209–215). Society for Mining, Metallurgy, and Exploration.

Smuts, E. M. (2015). *Methodology for CFD–DEM modelling of particulate suspension rheology* [PhD thesis]. University of Cape Town.

Van Lew, J. T., Park, Y. H., Ying, A., & Abdou, M. (2015). Modifying Young's modulus in DEM simulations based on distributions of experimental measurements. *Fusion Engineering and Design, 98–99*, 1893–1897. https://doi.org/10.1016/j.fusengdes.2015.06.012

Yan, Z., Wilkinson, S. K., Stitt, E. H., & Marigo, M. (2015). Discrete element modelling (DEM) input parameters: Understanding their impact on model predictions using statistical analysis. *Computational Particle Mechanics, 2*, 283–299. https://doi.org/10.1007/s40571-015-0056-5

Zhai, J., Chen, P., Sun, W., Chen, W., & Wan, S. (2022). A review of mineral processing of ilmenite by flotation. *Minerals Engineering, 157*, 106558. https://doi.org/10.1016/j.mineng.2020.106558

Zhu, H. P., Zhou, Z. Y., Yang, R. Y., & Yu, A. B. (2008). Discrete particle simulation of particulate systems: A review of major applications and findings. *Chemical Engineering Science, 63*, 5728−5770. https://doi.org/10.1016/j.ces.2008.08.006